

Astronomy & Astrophysics manuscript no.
 (will be inserted by hand later)

RXTE broadband X-ray spectra of intermediate polars and white dwarf mass estimates

V. Suleimanov^{1,2}, M. Revnivtsev^{2,3}, and H. Ritter²

¹ Kazan State University, Kremlevskaya str.18, 420008 Kazan, Russia

² Max-Planck-Institut für Astrophysik, Karl-Schwarzschild-Str. 1, D-85740 Garching bei München, Germany

³ Space Research Institute, Russian Academy of Sciences, Profsoyuznaya 84/32, 117810 Moscow, Russia

Received May 13, 2004

Abstract. We present results of an analysis of broadband spectra of 14 intermediate polars obtained with the RXTE observatory (PCA and HEXTE spectrometers, 3-100 keV). By means of our calculations of the structure and the emergent spectrum of the post-shock region of intermediate polars we fitted the observed spectra and obtained estimates of the white dwarf masses. The estimated masses are compared with masses obtained by other authors.

Key words. stars: binaries: close – stars: binaries: spectroscopic – stars: binaries: X-ray – stars: novae, cataclysmic variables

1. Introduction

Intermediate polars (IP) form a sub-class of magnetic cataclysmic variables (mCV) (Warner 1995). A white dwarf (WD) accretes matter from a companion star (typically a red dwarf) that fills its Roche lobe. This matter forms an accretion disc inside the Roche lobe of the primary which, however, is disrupted by the WD magnetic field at some distance from the WD surface. As a result the accreting matter freely falls on to the WD surface and forms a strong shock near its surface. The post-shock matter has a high temperature ($\sim 10\text{--}20$ keV) and emits X-rays via optical thin thermal plasma emission (Lamb & Masters 1979).

The temperature of the post-shock matter depends on the WD mass and therefore the X-ray spectra of IPs can be used for WD mass determination (Rothschild et al. 1981). Ishida (1991) had estimated the masses of the WDs of IPs and polars by using GINGA/LAC observations. He fitted the X-ray spectra by single temperature bremsstrahlung model. Then WD masses were estimated by equaling the resulting best fit bresstrahlung temperatures to the maximal shock temperatures. In reality a significant part of the post-shock region has smaller temperatures due to radiative cooling and, as mentioned by the author, WD masses obtained in this way are lower limits only.

In order to estimate the masses of WDs more carefully by using X-ray spectra of IPs one needs to calculate the temperature and emissivity distribution in the post-shock region (PSR). The structure of the PSR was investigated

by Aizu (1973), Wu et al. (1994), Woelk & Beuermann (1996), Cropper et al. (1999), see also Frank, King & Raine (2002). Wu et al. (1994) and Woelk & Beuermann (1996) took into account cyclotron cooling, which can be important for polars. In these papers it was shown that cyclotron cooling is not important for IPs if the surface magnetic field is less than ≈ 10 MG. The model of Wu et al. (1994) was used by Cropper et al. (1998, 1999) for fitting the spectra of IPs observed by GINGA/LAC and by Ramsay (2000) for fitting the spectra of IPs observed by RXTE/PCA. Beardmore et al. (2000) used the results of a simple analytical model of the PSR (see Frank, King & Raine 2002) for a comparison with the spectra of V1223 Sgr observed by GINGA/LAC and ASCA. Ezucka and Ishida (1999) estimated the WD masses of nine IPs using emission line ratios from ASCA observations.

The main systematic uncertainty in these works is caused by the fact that neither the GINGA/LAC nor the RXTE/PCA detectors provide adequate information at energies $>20\text{--}25$ keV. Therefore, it is hard to get solid estimates for the masses of the WDs if the mass is $> 0.6 M_{\odot}$, because in that case the maximal post-shock temperature is > 20 keV.

In this work we present results of WD mass estimates for 14 bright IPs, obtained from broad-band (3-100 keV) RXTE spectra. Most of the sources analized have a statistically significant signal at energies >10 keV. The observed spectra have been fitted by PSR model spectra. We compare the WD masses resulting from our best fit

parameters with the WD masses that were obtained by other methods.

2. The model

The structure of the stationary post-shock region in plane-parallel one-dimensional geometry is described (see e.g. Cropper et al. 1999) by the mass continuity equation

$$\frac{d}{dz}(\rho v) = 0, \quad (1)$$

the momentum equation

$$\frac{d}{dz}(\rho v^2 + P) = -\frac{GM_{wd}}{z^2} \rho, \quad (2)$$

the energy equation

$$v \frac{dP}{dz} + \gamma P \frac{dv}{dz} = -(\gamma - 1)\Lambda, \quad (3)$$

and the ideal-gas law

$$P = \frac{\rho k T}{\mu m_H}. \quad (4)$$

Here z is spatial coordinate (see Fig.1), v is the velocity of matter, ρ is the density, T is the temperature, P the gas pressure, $\gamma=5/3$ the adiabatic index, and $\mu=0.62$ the mean molecular weight of fully ionized matter of solar composition. The cooling rate Λ due to thermal optically thin radiation is:

$$\Lambda = \left(\frac{\rho}{\mu m_H} \right)^2 \Lambda_N(T), \quad (5)$$

where $\Lambda_N(T)$ is the cooling function, here taken for solar chemical composition as calculated and tabulated by Sutherland and Dopita (1993).

Equation (1) has the integral

$$\rho v = a, \quad (6)$$

where a is the local mass accretion rate per unit area (of dimension $\text{g cm}^{-2} \text{s}^{-1}$). The local mass accretion rate is a free parameter of the model. However, we found that the spectrum of emergent radiation is rather insensitive to this parameter within reasonable limits (i.e. as long as the emission region is optically thin with respect to free-free scattering).

Equations (2) and (3) can be rewritten using (6) with the substitution $z' = z_0 - z$, where z_0 is the shock coordinate (see Fig. 1):

$$\frac{dv}{dz'} = g(z') \frac{1}{v} - \frac{1}{a} \frac{dP}{dz'}, \quad (7)$$

$$\frac{dP}{dz'} = \frac{(\gamma - 1)\Lambda a + g(z')\gamma Pa/v}{\gamma P - av}, \quad (8)$$

where

$$g(z') = \frac{GM_{wd}}{(z_0 - z')^2}. \quad (9)$$

Equations (7) and (8) were solved by the shooting method from $z = z_0$ ($z' = 0$) to $z = R_{wd}$ ($z' = z_0 - R_{wd}$) with boundary conditions at $z = z_0$:

$$v_0 = 0.25 \sqrt{2GM_{wd}/z_0}, \quad (10)$$

$$\rho_0 = \frac{a}{v_0}, \quad (11)$$

$$P_0 = 3av_0, \quad (12)$$

$$T_0 = 3 \frac{\mu m_H}{k} v_0^2. \quad (13)$$

The WD radius was calculated from the Nauenberg (1972) WD mass-radius relation:

$$R_{wd} = 7.8 \cdot 10^8 \text{ cm} \times \left[\left(\frac{1.44M_\odot}{M_{wd}} \right)^{2/3} - \left(\frac{M_{wd}}{1.44M_\odot} \right)^{2/3} \right]^{1/2}.$$

In Fig.2 we present the temperature and the density profiles of the post-shock region resulting from our model for a particular set of boundary values. For comparison we show the profiles obtained by the simple analytical model (Frank, King & Raine 2002):

$$T(z) = T_0 \left(\frac{z - R_{wd}}{z_0 - R_{wd}} \right)^{2/5}, \quad (14)$$

$$\rho(z) = \rho_0 \left(\frac{z - R_{wd}}{z_0 - R_{wd}} \right)^{-2/5}. \quad (15)$$

This model is based on the assumption of constant pressure in the post-shock region. In our model the pressure grows towards WD surface, therefore the temperature and the density in our model are larger.

As the RXTE/PCA detectors have relatively poor spectral resolution and have sensitivity only at energies higher than 3 keV we limited ourself to the study of the continuum emission. The emergent lines at energies 6-7 keV in the resulting spectrum were mimicked by broad gaussian lines.

The emergent model spectrum is calculated by summing of the local bremsstrahlung spectra:

$$F_E = \int_{R_{wd}}^{z_0} j(z) dz, \quad (16)$$

where the local spectra were taken in the following form (Zombeck 1990):

$$j(z) = 9.52 \cdot 10^{-38} \times \left(\frac{\rho(z)}{\mu m_H} \right)^2 T(z)^{-1/2} \left(\frac{E}{kT(z)} \right)^{-0.4} \exp \left(-\frac{E}{kT(z)} \right).$$

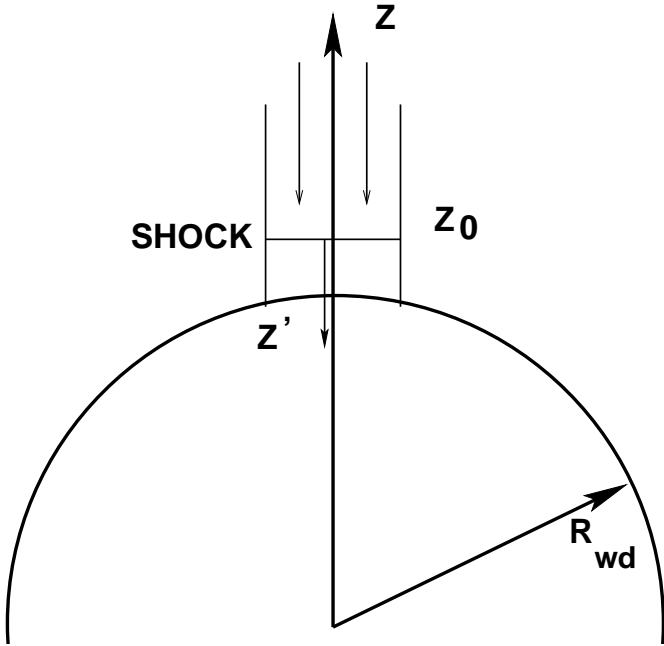


Fig. 1. . Geometry of a post-shock region model.

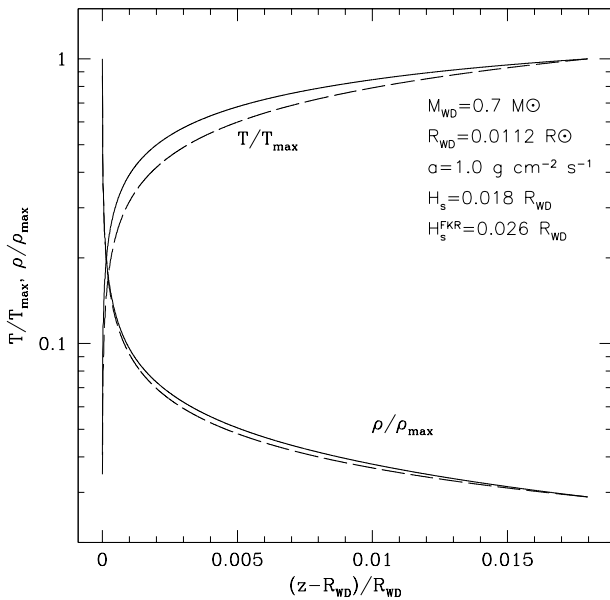


Fig. 2. . Temperature and density profiles for one of the PSR models. Dashed lines denote simplistic analytic solution of the structure of post-shock region (Frank, King & Raine 2002)

3. Observations and data reductions

In order to compare the results of our model calculations with observations we have chosen the data of the RXTE observatory that cover a relatively broad energy band (3–250 keV), where IPs release most of their emission. We

limited ourselves only to relatively bright IPs, as we are interested in the hard X-ray (>20 keV) part of the spectra of IPs. The list of IPs consists of V1223 Sgr, FO Aqr, EX Hya, AO Psc, TV Col, GK Per, V709 Cas, PQ Gem, V2400 Oph, BG CMi, V405 Aur, V1062 Tau, DO Dra, TX Col.

The data of the RXTE/PCA and the RXTE/HEXTE were reduced by means of standard tasks of the LHEASOFT/FTOOLS 5.2 package. The background subtraction of the PCA detectors was done with the CMI7_240 model. The subtraction of the background of the HEXTE detectors is especially important in our case which concentrates on the hard X-ray part of the spectrum of IPs. In order to monitor the background of the detectors the HEXTE is rocking by $\pm 1.5^\circ$ with respect to the target. We analysed the HEXTE spectra of IPs only if the background spectra obtained at the $+1.5^\circ$ and the -1.5° offset positions were statistically compatible, in other words if there were no contaminating sources in the vicinity of our targets.

4. Results

The spectra of the 14 IPs, extracted from the RXTE data are presented in Figs. 3 – 5.

For fitting these spectra we used results of our model calculations described in the previous section with one or two (only in the case of very bright IPs V1223 Sgr and GK Per) partial covering components. In contrast to the model used by Cropper et al. (1998) our model lacks the reflected component. However, as has been shown by Cropper et al. (1998) taking into account the reflection changes the best fit parameters and thus the WD mass only slightly. In addition to that, the usage of spectral information at energies higher than ~ 20 keV helps us to further reduce the influence of the reflected component on the shape of the spectral cutoff.

The best fit parameters resulting from our model are presented in Table 1. Using the observed and absorption-corrected fluxes of IPs we estimated their luminosities and mass accretion rates. The best fit model is shown in Figs. 3 – 5 by a solid line.

We compare the resulting estimates of WD masses with those measured by other methods. In the catalog of Cataclysmic Variables (Ritter & Kolb 2003) there are only 5 intermediate polars that have a spectroscopically measured mass. On Fig. 6 we present a comparison of our mass estimates with those given in the catalog. It is seen that we have a relatively good agreement, however the error bars of all these estimates are quite large. The only system that likely has a higher mass than we obtained from our X-ray spectral modelling is GK Per (during outburst). One possible explanation of this fact could be the WD's fast rotation ($P_{\text{sp}} = 351$ s). It is well known that the radius of the magnetosphere in systems with an accretion disc depends on the mass accretion rate. If the WD in GK Per is rotating close to its equilibrium period in its quiescent state (i.e. if the radius of its magnetosphere

Table 1. Best fit model parameters and inferred physical system parameters. Here C_F the partial covering coefficient, F_{3-100} the observed X-ray flux in the band 3 – 100 keV, $F_{0.1-100}$ the unabsorbed X-ray flux in the band 0.1 – 100 keV, both in 10^{-11} erg cm $^{-2}$ s $^{-1}$ units. Distances for V405 Aur, V709 Cas, PQ Gem and V2400 Oph are assumed.

Name	M_{wd}, M_\odot	C_F	$N_H, 10^{22} \text{cm}^{-2}$	F_{3-100}	$F_{0.1-100}$	$\dot{M} 10^{16} \text{g s}^{-1}$	$L_x 10^{33} \text{erg s}^{-1}$	d pc
V1223 Sgr	0.95 ± 0.05	1.0^a 0.57 ± 0.05	3.7 ± 1 28 ± 3	4.2	7.3	12.6	24.3	527 ¹
FO Aqr	0.6 ± 0.05	0.9 ± 0.1	36 ± 4	1.5	4.9	10.2	9.4	400 ²
EX Hya	0.5 ± 0.05	1.0	0.6 ± 1.0	1.5	3.4	0.25	0.17	64.5 ³
AO Psc	0.65 ± 0.05	0.95 ± 0.1	10 ± 5	1.3	2.5	4.7	4.9	420 ⁴
TV Col	0.84	0.81	21	1.7	3.5	3.4	5.7	368 ⁵
GK Per	0.59 ± 0.05	1.0^a 0.75 ± 0.05	20 ± 2 125 ± 10	12.5	88.6	81.5	156	340 ⁶
V709 Cas	0.9 ± 0.1	0.5 ± 0.1	29 ± 5	2.3	3.7	5.76	11.1	(500)
PQ Gem	0.65 ± 0.2	1.0	5 ± 1	0.80	1.3	3.7	3.9	(500)
V2400 Oph	0.59 ± 0.05	0.4 ± 0.1	29 ± 10	2.43	5.6	18.7	16.75	(500)
BG CMi	0.85 ± 0.12	0.70 ± 0.05	25 ± 6	0.77	1.54	5.3	9.0	700 ⁷
V405 Aur	0.9 ± 0.1	0.6 ± 0.1	39 ± 3	0.9	1.7	2.65	5.09	(500)
V1062 Tau	1.0 ± 0.2	0.6 ± 0.1	21 ± 7	1.1	1.8	2.2	5.4	500 ⁸
DO Dra	0.75 ± 0.05	0.4 ± 0.1	20 ± 5	7.8	14.4	3.1	4.1	155 ⁹
TX Col	0.7 ± 0.3	< 0.4	< 60	0.32	0.58	1.8	2.1	550 ¹⁰

^a – for systems V1223 Sgr and GK Per which have very high mass accretion rates we used two absorbers.

References to distance estimates: 1. Beuermann et al. (2004), 2. McHardy et al. 1987 3. Beuermann et al. 2003, 4. Hellier, Cropper & Mason 1991, 5. McArtur et al. 2001, 6. Warner 1987, 7. Berriman 1987, 8. Szkody & Silber 1996, 9. Mateo, Szkody & Garnavich 1991, 10. Buckley & Tuohy 1989

Table 2. Comparison of mass estimates obtained in this work with those obtained with the usage of other X-ray instruments

Name	PCA+HEXTE M_\odot	RXTE/PCA M_\odot	Ginga M_\odot	ASCA M_\odot
V1223 Sgr	0.9	1.1		1.28
FO Aqr	0.6	0.88	0.92	1.05
EX Hya	0.5	0.45	0.46	0.48
AO Psc	0.65	0.60	0.56	0.40
TV Col	0.84	0.96	1.30	0.51
GK Per	0.59			0.52
V709 Cas	0.9	1.08		
PQ Gem	0.65			
V2400 Oph	0.59	0.71		0.68
BG CMi	0.85	1.20	1.09	
V405 Aur	0.9	1.10		>0.54
V1062 Tau	1.0	0.90		
DO Dra	0.75			
TX Col	0.7	0.73	0.48	0.66

is close to the corotation radius) then it means that during an outburst (increase of the mass accretion rate by a factor of 10–20, see Ishida et al. 1992) the size of the magnetosphere should shrink by a factor of ~ 2 . Therefore the radius of the magnetosphere in GK Per during an outburst can be as small as $2 - 3 \times 10^9$ cm, and thus, only a factor of 5–8 larger than the radius of the WD. In this case the free fall velocity gained by the accreting matter near the surface of the WD will be somewhat smaller than in the case of falling from infinity (our model assumption).

Therefore the mass of the WD could be underestimated by as much as 10–20%.

Note that our mass estimates are in better agreement with those obtained from optical methods than those obtained by Cropper et al. (1999) from their analysis of the GINGA/LAC X-ray spectra (\sim 2–20 keV) (see Table 2). The masses obtained by Ramsay 2000 from his analysis of the RXTE/PCA (\sim 2–20 keV) spectra are closer to our estimates, but also slightly higher. A possible reason for this difference could be the lack of the hard X-ray part in the observed spectra.

It is interesting to mention that the parameters in our Table 1 show a correlation of the mass accretion rate with the strength of photoabsorption, that, in principle, is anticipated for IPs because systems with higher mass accretion rates have higher N_H values. A similar effect was observed in the case of GK Per (quiescent and outburst spectra) by Ishida et al. (1992).

5. Conclusions

Estimating the masses of the WDs in cataclysmic variables is a relatively complicated problem. The standard method based on radial velocity measurements often gives unreliable results because of our poor knowledge of the inclination angle of the binary system. Besides, spectral lines from accretion discs are very broad in comparison with Doppler shifts caused by orbital motion and their emissivity distributions can be non-axisymmetric (in the frame of reference of the WD). Therefore, additional assumptions, such as a relation between the mass of the secondary star

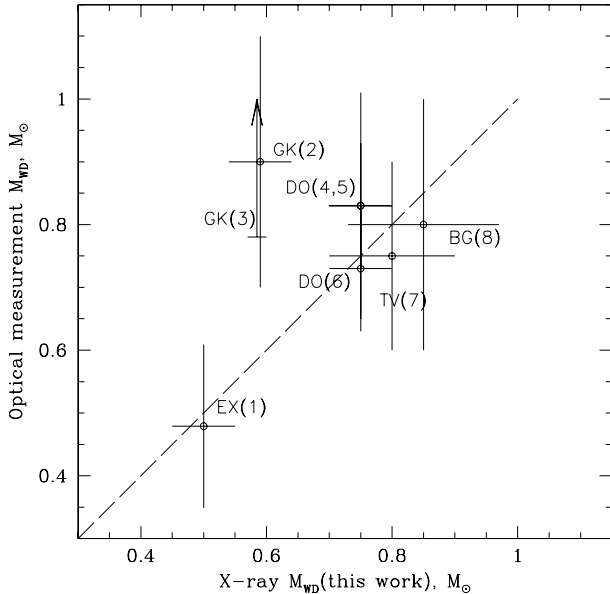


Fig. 6. Comparison of the masses of the white dwarfs as estimated from the RXTE broadband spectra (this work) with estimates obtained by other methods. (1) - Beuermann et al. (2003), (2) - Crampton et al. (1986), (3) - Reinsch (1994), (4) - Haswell et al. (1997), (5) - Mateo et al. (1991), (6) - Friend et al. (1990), (7) - Hellier (1993), (8) - Penning (1985)

and the orbital period (based on a mass-radius relation for main sequence stars, see Warner 1995) are often used.

Magnetic cataclysmic variables provide us with an additional way for estimating the masses of the WDs. The matter accreted onto the WD surface is heated in a standing shock and the maximal temperature of the plasma after the shock front depends practically on WD mass only. Therefore it is possible to estimate WD masses in polars and intermediate polars by fitting their X-ray spectra with model spectra of the radiation emerging from the post-shock region. If both methods of mass determinations are available it is very interesting to compare the resulting mass estimates. The temperatures of the PSR are relatively high (10 – 30 keV). Therefore the study of WD spectra in standard X-ray band suffers from a lack of information at energies of a few $\times kT$, that would strongly help to constrain the WD mass estimate.

In this work we present the WD masses of 14 IPs estimated from fitting the broad band (3-100 keV) RXTE/PCA+HEXTE X-ray spectra with model spectra of the PSR. We did not take into account cyclotron cooling of the PSR and therefore did not consider polars, where it can be important. Our estimates of WD masses are smaller than those obtained from GINGA/LAC (Cropper et al. 1999) and RXTE/PCA (Ramsay 2000) data. We also find

satisfactory agreement between our WD mass estimates and those obtained by optical spectroscopic methods. We conclude that it is necessary to include the hard X-ray spectral band ($E > 20$ keV) for obtaining reliable WD mass estimates in mCVs.

Acknowledgements. The work was supported by the Russian Foundation of Fundamental Research (grant 02-02-17174), by the President programm for support of leading science school (grant NSh - 1789.2003.2), by grants of Minpromnauka NSh-2083.2003.2 and 40.022.1.1.1103 and program of Russian Academy of Sciences “Non-stationary phenomena in astronomy”. Research has made use of data obtained from High Energy Astrophysics Science Archive Research Center Online Service, provided by the NASA/Goddard Space Flight Center.

References

- Aizu K. 1973, Prog. Theor. Phys., 49, 1184
- Beardmore, A., Osborne, J., Hellier, C. 2000, MNRAS, 315, 307
- Berriman G. 1987, A&A , 412, 821
- Beuermann K., Harrison Th., McArthur B., Benedict G., Gänsicke B. 2003, A&A , 412, 821
- Beuermann K., Harrison Th., McArthur B., Benedict G., Gänsicke B. 2004, A&A in press, astro-ph/0402548
- Buckley D.A.H. & Tuohy I.R. 1989, ApJ , 344, 376
- Crampton D., Cowley A.P., Fisher W.A., 1986, ApJ, 300, 788
- Cropper M., Ramsay G., Wu K. 1998, MNRAS, 293, 222
- Cropper M., Wu K., Ramsay G., Kocabiyik A. 1999, MNRAS, 306, 684
- Ezuka H., Ishida M. 1999, ApJS, 120, 277
- Frank J., King A., Raine D., 2002, Accretion Power in Astrophysics, Cambridge Univ. Press, Cambridge, 3rd edition
- Friend, M.T., Martin, J.S., Smith, R.C., Jones, D.H.P. 1990, MNRAS, 246, 637
- Haswell, C.A., Patterson, J., Thorstensen, J.R., Hellier, C., Skillman, D.R. 1997, ApJ, 476, 847
- Hellier C., Cropper M., Mason K. 1991, MNRAS, 248, 233
- Hellier C. 1993, MNRAS, 264, 132
- Ishida M. 1991, Ph.D. thesis, Univ. of Tokio
- Ishida M., Sakao, T., Makishima, K. et al. 1992, MNRAS, 254, 647
- Lamb D., Masters A. 1979, ApJ, 234, L117
- Mateo M., Szcodry P., Garnavich P. 1991, ApJ, 370, 370
- McArthur, B.E., Benedict, G.F., Lee, J. et al. 2001, ApJ, 560, 907
- McHardy I. M., Pye J.P., Fairall A., Menzies J. 1987, MNRAS, 225, 355
- Nauenberg M. 1972, ApJ, 175, 417
- Penning 1985, ApJ, 289, 300
- Ramsay G. 2000, MNRAS, 314, 403
- Reinsch K. 1994, A&A, 281, 108
- Ritter H., Kolb U. 2003, A&AS, 404, 301
- Rothschild, R. E., Gruber, D. E., Knight, F. K. et al. 1981, ApJ, 250, 723
- Szkody, P., Silber, A. 1996, AJ, 112, 289
- Sutherland, R. S., Dopita, M. A. 1993, ApJS, 88, 253
- Warner B. 1987, MNRAS, 227, 23
- Warner B. 1995, Cataclysmic variable stars, Cambridge Univ. Press, Cambridge
- Woelk U., Beuermann K. 1996, A&A, 306, 232

Wu K., Chanmugam G., Shaviv G. 1994, ApJ, 426, 664
Zombeck M.V. 1990, Handbook of Astronomy and
Astrophysics, Cambridge Univ. Press, Cambridge

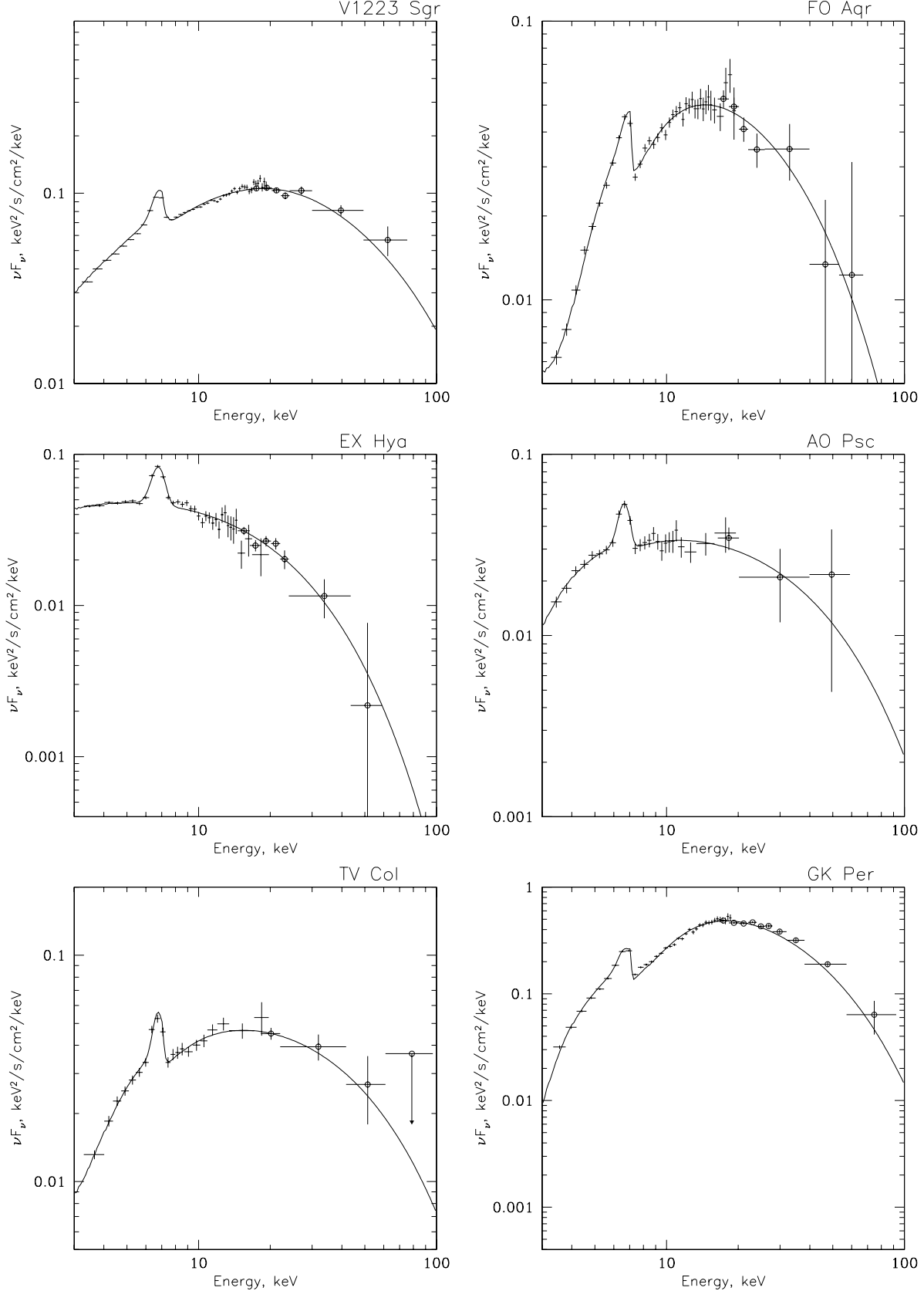
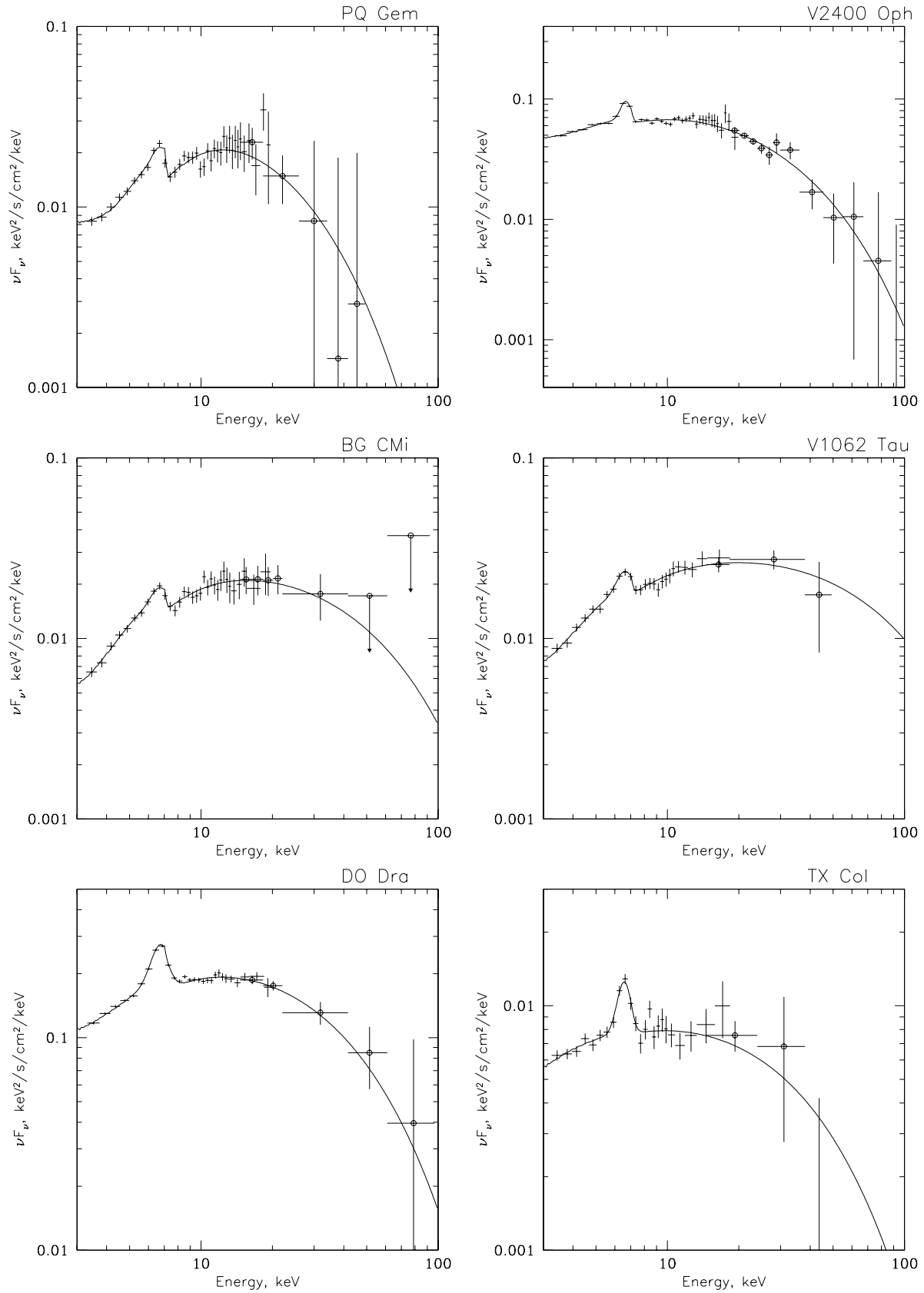


Fig. 3. Spectra of intermediate polars obtained with the RXTE observatory. Crosses denote the PCA data, open circles - HEXTE data. Solid lines show best fit model with parameters presented in Table 1

**Fig. 4.** The same as Fig. 3

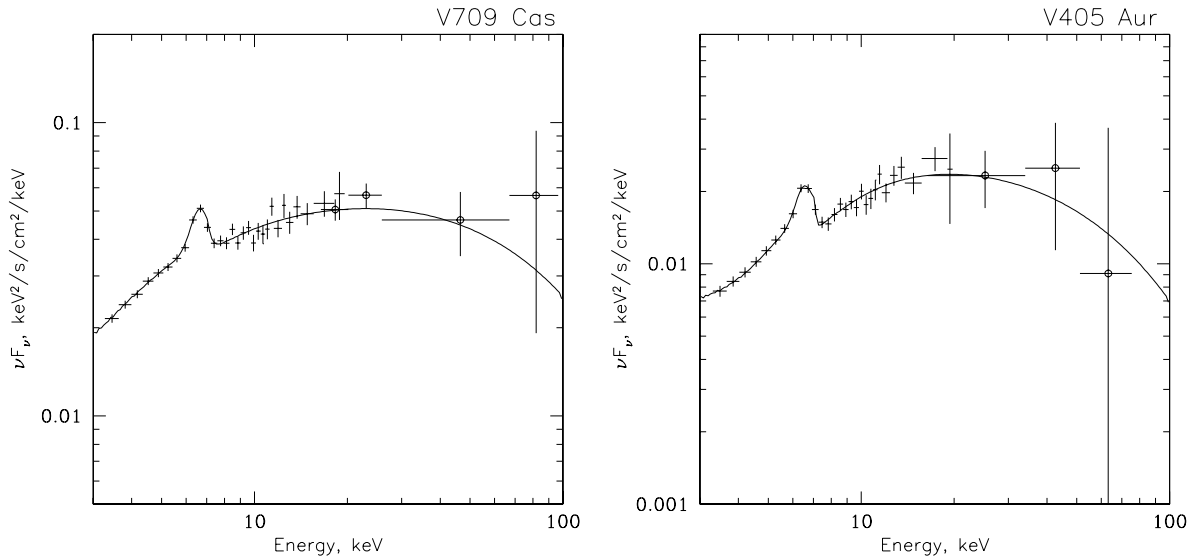


Fig. 5. The same as Fig. 3